ACS APPLIED MATERIALS & INTERFACES

Letter

www.acsami.org

Immobilization on Metal–Organic Framework Engenders High Sensitivity for Enzymatic Electrochemical Detection

Cheng Zhang,[†] Xuerui Wang,[†] Miao Hou,[†] Xiaoyang Li,[†] Xiaoling Wu,[†] and Jun Ge*[,†]

[†]Key Lab for Industrial Biocatalysis, Ministry of Education, Department of Chemical Engineering, Tsinghua University, Beijing 100084, China

Supporting Information

ABSTRACT: The protection effect of metal–organic framework (MOF) provides high stability for immobilized enzyme. The small cavities of MOFs, however, usually result in decreased apparent substrate affinity and enzymatic activity of immobilized enzyme, compared to native enzyme. We synthesized zeolitic imidazolate framework-8 (ZIF-8) with a combination of mesoporous and microporous channels for cytochrome *c* (Cyt *c*) immobilization. Compared with native Cyt *c*, the immobilized Cyt *c* displayed increased apparent substrate affinity (Michaelis constant K_m reduced by ~50%), ~128% increased enzymatic activity, and 1.4-fold increased sensitivity in the enzymatic electrochemical detection of H_2O_2. The immobilized Cyt *c*-coated screen-printed electrode was applied for the fast detection of residual H_2O_2 in microliter food samples such as milk and beer, making it promising for the development of efficient biosensors.

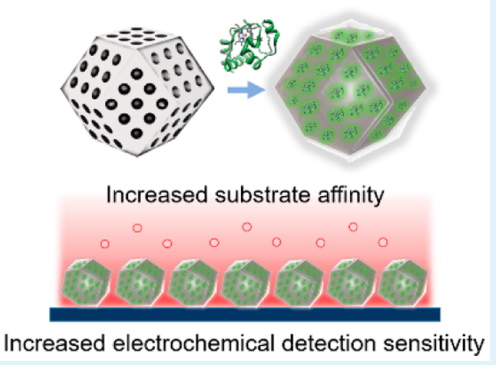

KEYWORDS: *metal-organic frameworks, enzyme immobilization, cytochrome c, electrochemical detection, biosensor*

A biosensor based on enzymatic electrochemical analysis is convenient and easily operated for highly sensitive and fast detection of targets in many application fields.[1−4] To improve the sensitivity of enzymatic electrochemical detection, researchers have majorly focused on enhancing the electron transfer efficiency between enzyme and electrode.[5−8] Little attention has been paid to increasing the apparent affinity between substrates and the immobilized enzymes on electrode. Theoretically, increasing the apparent substrate affinity (indicated by a reduced apparent Michaelis constant K_m of enzymatic reaction) of the immobilized enzyme should be another effective route to improving detection sensitivity.

However, although immobilized enzymes have enhanced stability,[9,10] they usually display lower apparent substrate affinity compared to native enzymes, largely due to the mass-transfer limitations imposed by immobilization carriers. Designing nanosized and porous carriers is an effective route to overcome the above limitation.[11,12] On the basis of this consideration, metal–organic frameworks (MOFs) as a type of excellent porous nanomaterials[13,14] have been investigated for enzyme immobilization by excellent pioneering research.[15−24] One strategy for immobilizing enzyme on MOFs is using special ligands to synthesize MOFs with large cavities (large enough for accommodating protein molecules), followed by the adsorption of enzyme.[15−17,20,22,23] The other strategy is the direct encapsulation of enzyme in zeolitic imidazolate frameworks (ZIFs), which can be achieved by the coprecipitation or biomimetic mineralization procedure.[18,19,21,24] In both cases, because of the protection effect of the rigid frameworks of MOFs, the stabilities of immobilized enzymes are greatly enhanced.[18−21] At the same time, the small cavities of MOFs, especially when using ZIFs, result in the unsmooth traffic of substrate to encapsulated enzyme and thus the decreased apparent substrate affinity of immobilized enzyme, which remains a challenge for enzyme immobilization on MOFs.

In this study, we reported the synthesis of zeolitic imidazolate frameworks-8 (ZIF-8) crystals with both mesoporous and microporous channels to immobilize enzyme with an improved apparent substrate affinity (Scheme 1). Previously, ZIF-8 has been reported as a promising carrier for enzyme immobilization because enzymes encapsulated in ZIF-8 usually have greatly increased enzyme stabilities.[18,21] Enzyme was located in the mesoporous channels, while the combination of mesoporous and microporous structure facilitated the substrate transportation. We immobilized cytochrome *c* (Cyt *c*), a low-cost protein compared to other peroxidases, on the ZIF-8, which can be oxidized by H_2O_2 and subsequently reduced by the electrode to achieve the electrochemical detection of H_2O_2. Detection of H_2O_2 is required in the food, pharmaceutical, and textile industries and in environmental protection.[25,26] As an additive for inhibiting the growth of microorganisms or bleaching in processing, H_2O_2 has been widely used in the food industry.[27] Because of the toxic effects of residual H_2O_2, the presence of H_2O_2 is not permitted in food under European Union and Japanese regulations.[28] A regulation of the Food and Drug Administration (FDA) limits residual H_2O_2 to 0.5 ppm.

Received: February 27, 2017
Accepted: April 11, 2017
Published: April 11, 2017

DOI: 10.1021/acsami.7b02803
ACS Appl. Mater. Interfaces 2017, 9, 13831−13836

Scheme 1. Synthesis of Cyt *c*@mesoZIF-8 and the Detection of H_2O_2 with Cyt *c*@mesoZIF-8/Screen-Printed Electrode (SPE)

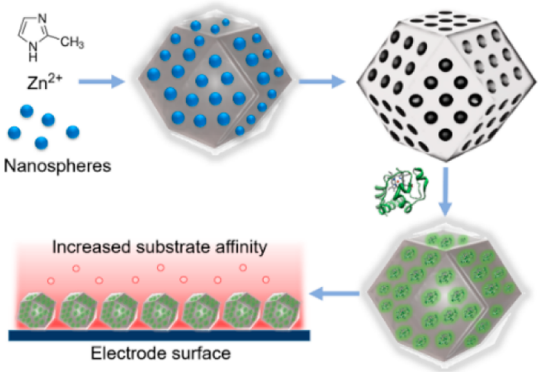

in finished food packages.[29] In this immobilization, the nanocarrier increases the substrate affinity and sensitivity of the enzymatic electrochemical analysis.

In a typical experiment, a water suspension of polystyrene (PS) nanospheres (50 nm, 1 g/mL, 50 μL), a methanol solution of zinc nitrate hexahydrate (25 mM, 50 mL), and a methanol solution of 2-methylimidazole (25 mM, 50 mL) were mixed at room temperature, followed by sonication for 1 h. The mixture was then incubated at room temperature for 24 h without stirring. The PS/ZIF-8 composites were obtained after 3 cycles of centrifugation and washing with methanol. The mesoporous ZIF-8 (mesoZIF-8) was then obtained by calcinating the PS/ZIF-8 composites at 350 °C for 3 h to remove PS nanospheres. Finally, the Cyt *c*@mesoZIF-8 composites were prepared by adsorbing Cyt *c* (1 mg/mL) on mesoZIF-8 (5 mg/mL) in phosphate buffer (50 mM, pH 7.4, 0.3 mg/mL polyvinylpyrrolidone). The immobilized enzyme was obtained by centrifugation and washing with water.

The scanning electron microscope (SEM) images (Figure 1a, b) proved the incorporation of PS nanospheres in ZIF-8. The loading percentage of PS nanospheres was about 9.3 wt %, determined by thermal gravimetric analyses (TGA) (Figure S1). The calcination generated mesopores (~50 nm) in ZIF-8 (Figure 1c). Protein molecules were observed to occupy the mesoporous channels of mesoZIF-8 on the surface (Figure 1d). The transmission electron microscope (TEM) images (Figure 1e–g) further confirmed the creation of mesoporous structures (the light electron density regions in Figure 1g indicated the mesoporous channels). The energy dispersive X-ray spectroscopy (EDS) mapping (Figure 1i, j) under TEM showed the existence and well-distribution of the S element (from amino

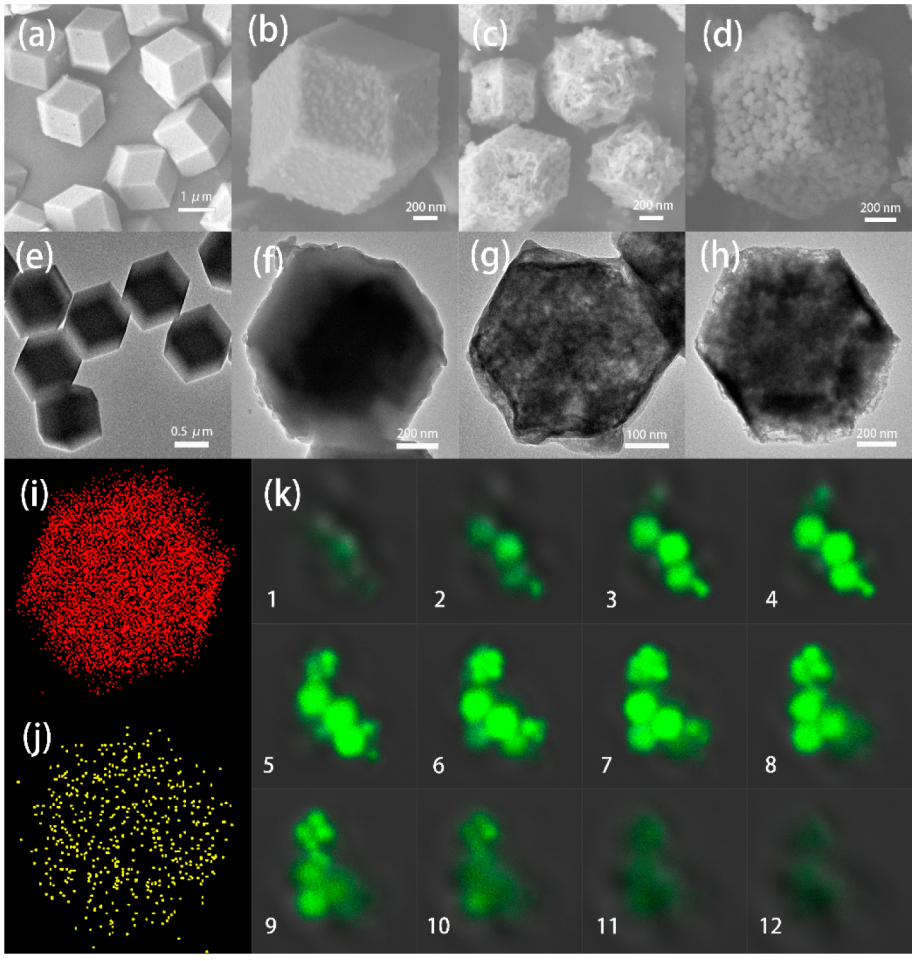

Figure 1. SEM images of (a) pure ZIF-8, (b) PS@ZIF-8 composites, (c) mesoZIF-8, (d) Cyt *c*@mesoZIF-8. TEM images of (e) pure ZIF-8, (f) PS@ZIF-8 composites, (g) mesoZIF-8, (h) Cyt *c*@mesoZIF-8. EDS mapping of elemental distributions of Cyt *c*@mesoZIF-8 for (i) Zn, (j) S. (k) Confocal laser scanning microscopy images of 12 continuous layers across 4.8 μm for FITC-labeled Cyt *c*@mesoZIF-8.

DOI: 10.1021/acsami.7b02803
ACS Appl. Mater. Interfaces 2017, 9, 13831–13836

acids of protein) in Cyt *c*@mesoZIF-8, proving the successful immobilization of Cyt *c*.

By labeling Cyt *c* with fluorescein isothiocyanate (FITC) and then immobilizing Cyt *c*-FITC on mesoZIF-8, the existence of Cyt *c*-FITC in the interior of mesoZIF-8 was observed under confocal laser scanning microscopy with different depths along z direction (Figure 1k). Because the micropores of mesoZIF-8 were much smaller than the size of Cyt c, the presence of protein in the interior of mesoZIF-8 suggested the mesopores might be connected, allowing protein molecules to transfer into the inside of mesoZIF-8. In addition, the BET analysis further demonstrated that after immobilization of Cyt *c*, most of the micropores and mesoporous channels of mesoZIF-8 cannot be detected because of the occupation by protein (Table S1 and Figure S11).

The PS@ZIF-8 composites, mesoZIF-8, and Cyt *c*@mesoZIF-8 displayed similar X-ray diffraction (XRD) patterns (Figure 2a) compared to pure ZIF-8, indicating the crystallinity was well-preserved. And after incubating in 0.3 wt % H_2O_2 for 15 min, the XRD pattern of Cyt *c*@mesoZIF-8 remained unchanged (Figure S2), indicating that H_2O_2 did not destroy the crystallinity of Cyt *c*@mesoZIF-8. The density functional theory (DFT) pore size distribution analysis of mesoZIF-8 gained by N_2 isotherms again revealed theco-existence of both micropores of ZIF-8 and mesopores (around 30−50 nm) generated by PS nanospheres (Figure 2b). The size of Cyt *c* is less than 10 nm, much smaller than the mesopores of mesoZIF-8, and thus it can easily be adsorbed into the mesoZIF-8.

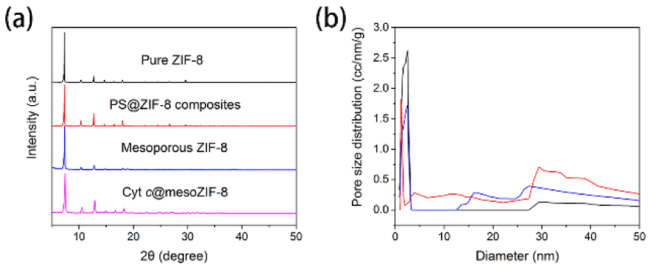

Figure 2. (a) XRD patterns of pure ZIF-8, PS@ZIF-8 composites, mesoZIF-8, and Cyt *c*@mesoZIF-8. (b) DFT pore size distributions for pure ZIF-8 (black), PS@ZIF-8 composites (blue), and mesoZIF-8 (red).

The loading percentage of Cyt *c* on mesoZIF-8 was determined as 7.1 wt % by TGA (Figure S2), which agreed well with the percentage (7.5 wt %) calculated from inductively coupled plasma mass spectrometry (ICP-MS). Since Cyt *c* has Fe element at its active site, the analysis of ICP-MS was based on the determination of Fe in Cyt *c*@mesoZIF-8 (see Supporting Information for standard curves and detailed results, Figures S16−S17, Table S2). In addition, the well agreement between TGA and ICP-MS suggested that there was no obvious adsorption of polyvinylpyrrolidone on Cyt *c*@mesoZIF-8 due to the washing step after synthesis. Polyvinylpyrrolidone utilized in the immobilization procedure served as a surfactant to better dissolve the relatively hydrophobic protein Cyt *c*. No leakage of protein was observed after keeping Cyt *c*@mesoZIF-8 in phosphate buffer solution for 1 week. In contrast, Cyt *c* adsorbed on native ZIF-8 crystals (without mesopores) exhibited a fast leakage in several hours, and after 36 h almost all Cyt *c* was unbound from ZIF-8 (Figure S4). Cyt *c* molecules can be physically adsorbed on the surface of ZIF-8 due to the electrostatic interaction. However, when incubating in aqueous solution, the physically adsorbed protein molecules were easily leaked from the surface of ZIF-8. In contrast, Cyt *c* immobilized on mesoZIF-8 were restricted in the mesoporous channels without an obvious leakage.

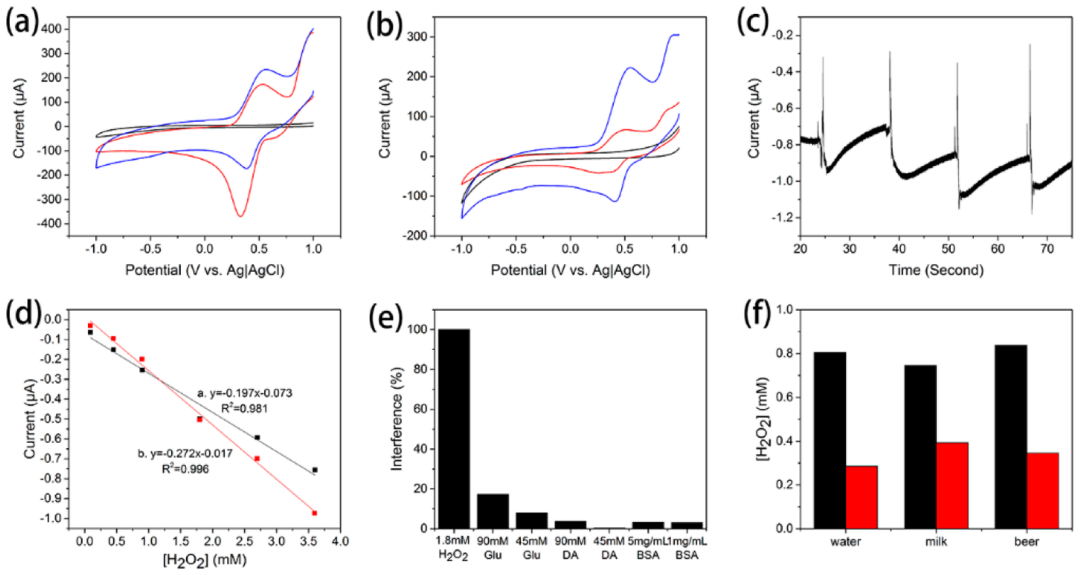

Figure 3. (a) Cyclic voltammograms for native Cyt *c*/SPE in PBS without ABTS (black), PBS in the presence of ABTS (red), PBS containing H_2O_2 and in the presence of ABTS (blue). (b) Cyclic voltammograms for Cyt *c*@mesoZIF-8/SPE in PBS without ABTS (black), PBS in the presence of ABTS (red), PBS containing H_2O_2 and in the presence of ABTS (blue). (c) Chronoamperometric response of Cyt *c*@mesoZIF-8/SPE with successive addition of 0.45 mM H_2O_2 at a constant potential of −0.05 V. (d) Calibration curve of the steady-state currents against concentrations of H_2O_2 for native Cyt *c*/SPE (black) and Cyt *c*@mesoZIF-8/SPE (red). (e) Selectivity of Cyt *c*@mesoZIF-8/SPE obtained at −0.05 V with the addition of H_2O_2, glucose (Glu), dopamine (DA) or bovine serum albumin (BSA). (f) Determination of H_2O_2 with the concentration of 0.8 mM (black) and 0.3 mM (red) in water, milk, and beer.

DOI: 10.1021/acsami.7b02803
ACS Appl. Mater. Interfaces 2017, 9, 13831−13836

The peroxidase activity of Cyt *c*@mesoZIF-8 was examined by the standard method using H_2O_2 and 2,2′-azino-bis (3-ethylbenzothiazoline-6-sulfonic acid) (ABTS) as substrates (see the Supporting Information for details). Compared with native Cyt *c*, Cyt *c*@mesoZIF-8 showed 128% activity, whereas ZIF-8 or mesoZIF-8 has no catalytic activity for H_2O_2, which was also proved by a previous study.[18] The apparent Michaelis constant K_m of Cyt *c*@mesoZIF-8, which indicated the affinity of the immobilized enzyme toward H_2O_2, was decreased to 7.4 mM from 13.7 mM for native Cyt *c* (Figures S5 and S6). Please note the decreased apparent K_m of Cyt *c*@mesoZIF-8 indicated that due to the porous structure of mesoZIF-8, the immobilized enzyme has a higher apparent affinity toward the substrate H_2O_2 compared to native Cyt *c*. In addition to the high activity and high substrate affinity, Cyt *c*@mesoZIF-8 displayed enhanced stability in the presence of H_2O_2. After incubation in 45 mM H_2O_2 for 15 min, native Cyt *c* lost almost all its original activity (Figure S7), whereas Cyt *c*@mesoZIF-8 still reserved more than 20% of activity.

The high activity and high apparent substrate affinity of Cyt *c*@mesoZIF-8 ensured its application in electrochemical detection of H_2O_2. Ten μL of ABTS water solution (5 mM), 10 μL of Cyt *c*@mesoZIF-8 water solution (10 μg Cyt *c*) and 2.5 μL of 1% Nanfion were coated on the screen-printed electrode (SPE) successively, to prepare the Cyt *c*@mesoZIF-8/SPE. As a control, native Cyt *c*/SPE was prepared using the same amount of protein and the same protocol. Typical cyclic voltammograms (CVs) (Figure 3a, b) were obtained by applying 100 μL of phosphate buffer saline (PBS) solution (with/without H_2O_2 or ABTS) on the electrode at a scanning rate of 0.5 V/s. The CVs of Cyt *c*/SPE and Cyt *c*@mesoZIF-8/SPE in pure PBS gave no redox peaks, indicating a poor electron transfer between the electrode and Cyt *c*. In the presence of ABTS, obvious peaks were observed, proving that ABTS can serve as an electron mediator. The CVs of Cyt *c*@mesoZIF-8/SPE and Cyt *c*/SPE with ABTS as the electron mediator in PBS containing 0.9 mM H_2O_2 showed cathodic peaks at 0.36 V. The cathodic peaks were responsible for the electrochemical reduction of Cyt *c* mediated by ABTS; the Cyt *c* molecules were previously oxidized by H_2O_2.[6,30]

For Cyt *c*@mesoZIF-8/SPE, the amperometric response (at the potential of −0.05 V) for successive addition of 0.45 mM H_2O_2 gave a linearly increase of absolute value (Figure 3c) upon each addition of H_2O_2. The amperometric response of Cyt *c*@mesoZIF-8/SPE and Cyt *c* /SPE in the detection of different concentrations of H_2O_2 was investigated (Figures S8 and S9). The detection linear ranges of both electrodes were extended from ∼0.09 mM to ∼3.6 mM H_2O_2 (Figure 3d). The sensitivity (represented by the slope of calibration curve) of Cyt *c*@mesoZIF-8/SPE was increased by 1.4 fold compared to that of native Cyt *c*/SPE (Figure 3d). Please note that the apparent K_m of Cyt *c*@mesoZIF-8 was significantly decreased compared to native Cyt *c*, which was described above. The decreased apparent K_m indicated an increased apparent substrate affinity of the immobilized enzyme. Here the increased apparent substrate affinity of Cyt *c*@mesoZIF-8/SPE toward H_2O_2 and high enzymatic activity resulted in the increased detection sensitivity. This result proved our hypothesis that the improved apparent substrate affinity of immobilized enzyme by MOFs increased the detection sensitivity of the enzyme electrode. Prepared by a polymer-assisted coprecipitation process in methanol,[18] the Cyt *c* embedded in ZIF-8 crystals had a similar decreased K_m, indicating an increased substrate affinity for H_2O_2. However, a further study of preparing various enzyme-encapsulated ZIF-8 composites in aqueous solution resulted in dramatically increased Km values suggesting the unsmooth traffic of substrates with relatively large molecular weights to the encapsulated enzymes.[19] In this study, because ABTS, which served as the electron mediator between the active site of Cyt *c* and the electrode, has much larger molecular weight than H_2O_2, small cavities of ZIF-8 restricted the contact of ABTS with encapsulated Cyt *c* and a combination of mesoporous and microporous channels of mesoZIF-8 enhanced the electrochemical detection. Compared with other immobilized Cyt *c*-modified electrodes reported in literature, Cyt *c*@mesoZIF-8/SPE showed a wide detection range, but its sensitivity was not as high as the electrodes modified with carbon nanotubes, graphene or nanogold (Table S3), which might be due to the low conductivity of ZIF-8 compared to nanostructured carbon or gold materials.

The Cyt *c*@mesoZIF-8/SPE displayed a high selectivity. The response current for glucose (Glu), dopamine (DA) and bovine serum albumin (BSA) with 50- and 25-fold high concentrations compared to H_2O_2 was given in Figure 3e. The response current of H_2O_2 was much higher than that of other interferences (even they were at much higher concentrations), demonstrating the good selectivity for H_2O_2. To demonstrate the application of the immobilized Cyt *c*-coated screen-printed electrode, we further tested the detection capability of Cyt *c*@mesoZIF-8/SPE in real food samples such as beer and milk. Beer or milk containing specific amounts of H_2O_2 was prepared by adding certain amounts H_2O_2 in the samples. Then, 100 μL of beer or milk containing H_2O_2 with different concentrations was dropped on the working area of Cyt *c*@mesoZIF-8/SPE. After applying a working potential of −0.05 V for 1 min, the response current was measured. As shown in Figure 3f, the concentrations of H_2O_2 in these food samples were accurately determined, agreeing well with the theoretical values and also fitting well with that of water solution containing the same amount of H_2O_2. Moreover, because the deactivation of Cyt *c* on electrode is very slow at room temperature, to investigate the storage stability of the enzyme electrode, we carried out the aging test of the enzyme electrode at 80 °C. As shown in Figure S10, after 1 h at 80 °C no obvious drop in the capability of electrochemical detection of H_2O_2 was observed for the Cyt *c*@mesoZIF-8/SPE. However, Cyt *c*/SPE lost half of its detection capability at the same condition. It is possible that the encapsulation of Cyt *c* in mesoporous channels well protected the protein configuration of Cyt *c*, resulting in a high enzyme stability.

In conclusion, mesoporous ZIF-8 was synthesized for Cyt *c* immobilization. The Cyt *c* on mesoporous ZIF-8 displayed 128% activity and much increased apparent substrate affinity, compared to native Cyt *c*. The high apparent substrate affinity made the immobilized enzyme ideal for fabrication of enzyme electrode with a high senility. The immobilized Cyt *c*-coated screen-printed electrode exhibited a 1.4-fold increased sensitivity in the detection of H_2O_2, compared to native Cyt *c*-coated electrode. The fast and accurate determination of H_2O_2 amount in food samples such as milk and beer demonstrated the appealing application of immobilized Cyt *c*-coated screen-printed electrode as an efficient biosensor.

DOI: 10.1021/acsami.7b02803
ACS Appl. Mater. Interfaces 2017, 9, 13831−13836

■ ASSOCIATED CONTENT

Supporting Information

The Supporting Information is available free of charge on the ACS Publications website at DOI: 10.1021/acsami.7b02803.

Materials and experimental details, TGA, XRD, BET analysis of all products and samples, determination of Michaelis constants and stabilities of enzyme samples, typical current response vs amperometric time, etc. (PDF)

■ AUTHOR INFORMATION

Corresponding Author

*E-mail: junge@mail.tsinghua.edu.cn.

ORCID

Jun Ge: 0000-0001-5503-8899

Notes

The authors declare no competing financial interest.

■ ACKNOWLEDGMENTS

This work was supported by the National Key Research and Development Plan of China (2016YFA0204300), the National Natural Science Foundation of China (21622603, 51573085).

■ REFERENCES

(1) Cahova, H.; Havran, L.; Brazdilova, P.; Pivonkova, H.; Pohl, R.; Fojta, M.; Hocek, M. Aminophenyl- and Nitrophenyl-Labeled Nucleoside Triphosphates: Synthesis, Enzymatic Incorporation, and Electrochemical Detection. *Angew. Chem., Int. Ed.* **2008**, *47*, 2059−2062.

(2) Liao, C.; Mak, C.; Zhang, M.; Chan, H. L. W.; Yan, F. Flexible Organic Electrochemical Transistors for Highly Selective Enzyme Biosensors and Used for Saliva Testing. *Adv. Mater.* **2015**, *27*, 676−681.

(3) Zeng, Q.; Cheng, J.; Tang, L.; Liu, X.; Liu, Y.; Li, J.; Jiang, J. Self-Assembled Graphene−Enzyme Hierarchical Nanostructures for Electrochemical Biosensing. *Adv. Funct. Mater.* **2010**, *20*, 3366−3372.

(4) Lutz, B. J.; Fan, Z. H.; Burgdorf, T.; Friedrich, B. Hydrogen Sensing by Enzyme-Catalyzed Electrochemical Detection. *Anal. Chem.* **2005**, *77*, 4969−4975.

(5) Zhou, J.; Liao, C.; Zhang, L.; Wang, Q.; Tian, Y. Molecular Hydrogel-Stabilized Enzyme with Facilitated Electron Transfer for Determination of H2O2 Released from Live Cells. *Anal. Chem.* **2014**, *86*, 4395−4401.

(6) Dinesh, B.; Mani, V.; Saraswathi, R.; Chen, S.-M. Direct Electrochemistry of Cytochrome c Immobilized on a Graphene Oxide−Carbon Nanotube Composite for Picomolar Detection of Hydrogen Peroxide. *RSC Adv.* **2014**, *4*, 28229−28237.

(7) Madasamy, T.; Santschi, C.; Martin, O. J. F. A Miniaturized Electrochemical Assay for Homocysteine Using Screen-printed Electrodes with Cytochrome c Anchored Gold Nanoparticles. *Analyst* **2015**, *140*, 6071−6078.

(8) Yuan, J.; Guo, W.; Wang, E. Utilizing a CdTe Quantum Dots-Enzyme Hybrid System for the Determination of Both Phenolic Compounds and Hydrogen Peroxide. *Anal. Chem.* **2008**, *80*, 1141−1145.

(9) Sheldon, R. A.; van Pelt, S. Enzyme Immobilisation in Biocatalysis: Why, What and How. *Chem. Soc. Rev.* **2013**, *42*, 6223−6235.

(10) Garcia-Galan, C.; Berenguer-Murcia, A.; Fernandez-Lafuente, R.; Rodrigues, R. C. Potential of Different Enzyme Immobilization Strategies to Improve Enzyme Performance. *Adv. Synth. Catal.* **2011**, *353*, 2885−2904.

(11) Zore, O. V.; Pattammattel, A.; Gnanaguru, S.; Kumar, C. V.; Kasi, R. M. Bienzyme−Polymer−Graphene Oxide Quaternary Hybrid Biocatalysts: Efficient Substrate Channeling under Chemically and Thermally Denaturing Conditions. *ACS Catal.* **2015**, *5*, 4979−4988.

(12) Novak, M. J.; Pattammattel, A.; Koshmerl, B.; Puglia, M.; Williams, C.; Kumar, C. V. Stable-on-the-Table" Enzymes: Engineering the Enzyme−Graphene Oxide Interface for Unprecedented Kinetic Stability of the Biocatalyst. *ACS Catal.* **2016**, *6*, 339−347.

(13) Furukawa, H.; Cordova, K. E.; O'Keeffe, M.; Yaghi, O. M. The Chemistry and Applications of Metal-Organic Frameworks. *Science* **2013**, *341* (6149), 1230444.

(14) Zhou, H.-C.; Long, J. R.; Yaghi, O. M. Introduction to Metal−Organic Frameworks. *Chem. Rev.* **2012**, *112*, 673−674.

(15) Lykourinou, V.; Chen, Y.; Wang, X.-S.; Meng, L.; Hoang, T.; Ming, L.-J.; Musselman, R. L.; Ma, S. Immobilization of MP-11 into a Mesoporous Metal-Organic Framework, MP-11@mesoMOF: A New Platform for Enzymatic Catalysis. *J. Am. Chem. Soc.* **2011**, *133*, 10382−10385.

(16) Deng, H.; Grunder, S.; Cordova, K. E.; Valente, C.; Furukawa, H.; Hmadeh, M.; Gándara, F.; Whalley, A. C.; Liu, Z.; Asahina, S.; Kazumori, H.; O'Keeffe, M.; Terasaki, O.; Stoddart, J. F.; Yaghi, O. M. Large-Pore Apertures in a Series of Metal-Organic Frameworks. *Science* **2012**, *336*, 1018−1023.

(17) Chen, Y.; Lykourinou, V.; Vetromile, C.; Hoang, T.; Ming, L.-J.; Larsen, R. W.; Ma, S. How Can Proteins Enter the Interior of a MOF? Investigation of Cytochrome c Translocation into a MOF Consisting of Mesoporous Cages with Microporous Windows. *J. Am. Chem. Soc.* **2012**, *134*, 13188−13191.

(18) Lyu, F.; Zhang, Y.; Zare, R. N.; Ge, J.; Liu, Z. One-Pot Synthesis of Protein-Embedded Metal−Organic Frameworks with Enhanced Biological Activities. *Nano Lett.* **2014**, *14*, 5761−5765.

(19) Wu, X.; Ge, J.; Yang, C.; Hou, M.; Liu, Z. Facile Synthesis of Multiple Enzyme-Containing Metal-Organic Frameworks in a BiomoleculeFriendly Environment. *Chem. Commun.* **2015**, *51*, 13408−13411.

(20) Feng, D.; Liu, T.-F.; Su, J.; Bosch, M.; Wei, Z.; Wan, W.; Yuan, D.; Chen, Y.-P.; Wang, X.; Wang, K.; Lian, X.; Gu, Z.-Y.; Park, J.; Zou, X.; Zhou, H. C. Stable Metal-Organic Frameworks Containing Single-Molecule Traps for Enzyme Encapsulation. *Nat. Commun.* **2015**, *6*, 5979.

(21) Mao, Y.; Li, J.; Cao, W.; Ying, Y.; Hu, P.; Liu, Y.; Sun, L.; Wang, H.; Jin, C.; Peng, X. General Incorporation of Diverse Components Inside Metal-Organic Framework Thin Films at Room Temperature. *Nat. Commun.* **2014**, *5*, 5532−5540.

(22) Li, P.; Moon, S.-Y.; Guelta, M. A.; Harvey, S. P.; Hupp, J. T.; Farha, O. K. Encapsulation of a Nerve Agent Detoxifying Enzyme by a Mesoporous Zirconium Metal-Organic Framework Engenders Thermal and Long-Term Stability. *J. Am. Chem. Soc.* **2016**, *138*, 8052−8055.

(23) Li, P.; Moon, S.-Y.; Guelta, M. A.; Lin, L.; Gomez-Gualdron, D. A.; Snurr, R. Q.; Harvey, S. P.; Hupp, J. T.; Farha, O. K. Nanosizing a Metal−Organic Framework Enzyme Carrier for Accelerating Nerve Agent Hydrolysis. *ACS Nano* **2016**, *10*, 9174−9182.

(24) Li, S.; Dharmarwardana, M.; Welch, R. P.; Ren, Y.; Thompson, C. M.; Smaldone, R. A.; Gassensmith, J. J. Template-Directed Synthesis of Porous and Protective Core-Shell Bionanoparticles. *Angew. Chem., Int. Ed.* **2016**, *55*, 10691−10696.

(25) Zhang, Y.; Bai, X.; Wang, X.; Shiu, K.-K.; Zhu, Y.; Jiang, H. Highly Sensitive Graphene−Pt Nanocomposites Amperometric Biosensor and Its Application in Living Cell H_2O_2 Detection. *Anal. Chem.* **2014**, *86*, 9459−9465.

(26) Jv, Y.; Li, B.; Cao, R. Positively-Charged Gold Nanoparticles as Peroxidiase Mimic and Their Application in Hydrogen Peroxide and Glucose Detection. *Chem. Commun.* **2010**, *46*, 8017−8019.

(27) Nascimento, C. F.; Santos, P. M.; Pereira-Filho, E. R.; Rocha, F. R. P. Recent Advances on Determination of Milk Adulterants. *Food Chem.* **2017**, *221*, 1232−1244.

(28) Hsu, C.-L.; Chang, K.-S.; Kuo, J.-C. Determination of Hydrogen Peroxide Residues in Aseptically Packaged Beverages Using an Amperometric Sensor Based on a Palladium Electrode. *Food Control* **2008**, *19*, 223−230.

DOI: 10.1021/acsami.7b02803
ACS Appl. Mater. Interfaces 2017, 9, 13831−13836

(29) Code of Federal Regulations, 21CFR178.1005.
(30) Suarez, G.; Santschi, C.; Martin, O. G. F.; Slaveykova, V. I. Biosensor Based on Chemically-Designed Anchorable Cytochrome c for the Detection of H_2O_2 Released by Aquatic Cells. *Biosens. Bioelectron.* **2013**, *42*, 385−390.

DOI: 10.1021/acsami.7b02803
ACS Appl. Mater. Interfaces 2017, 9, 13831−13836